C. R. Chimie 17 (2014) 1237–1241

Contents lists available at ScienceDirect

Comptes Rendus Chimie

www.sciencedirect.com

Full paper/Mémoire

Study of the ionic conductivity of $Ca_6La_4(PO_4)_2(SiO_4)_4F_2$ and $Ca_4La_6(SiO_4)_6F_2$

Étude de la conductivité ionique de $Ca_6La_4(PO_4)_2(SiO_4)_4F_2$ et $Ca_4La_6(SiO_4)_6F_2$

Hela Njema, Khaled Boughzala, Anis Chaabène, Khaled Bouzouita *

Institut préparatoire aux études d'ingénieur de Monastir, 5019 Monastir, Tunisia

ARTICLE INFO

Article history:
Received 26 October 2013
Accepted after revision 18 February 2014
Available online 3 October 2014

Keywords:
Apatite
Lanthanum
Impedance spectroscopy
Ionic conductivity

Mots clés :
Apatite
Lanthane
Spectroscopie d'impédance
Conductivité ionique

ABSTRACT

In order to enhance our knowledge about the $Ca_{10-x}La_x(PO_4)_{6-x}(SiO_4)_xF_2$ ($0 \le x \le 6$) series, whose chemical stability decreases as the substitution degree increases, $Ca_6La_4(PO_4)_2(SiO_4)_4F_2$ and $Ca_4La_6(SiO_4)_6F_2$ compounds were prepared through a solid-state reaction. Their ionic conductivity was measured by impedance spectroscopy. The results indicate that the conductivity increases with substitution, and fits the Arrhenius equation over the investigated temperature range. At high temperatures, a change in the activation energy has been observed, which has been related to the nature of the Ca/La–F bond, i.e. to the polarizability of lanthanum.

RÉSUMÉ

Dans le but d'améliorer nos connaissances sur la série $Ca_{10-x}La_x(PO_4)_{6-x}(SiO_4)_xF_2$ ($0 \le x \le 6$), dont la stabilité chimique diminue lorsque le degré de substitution augmente, les composés $Ca_6La_4(PO_4)_2(SiO_4)_4F_2$ et $Ca_4La_6(SiO_4)_6F_2$ ont été synthétisés par réaction à l'état solide. Leur conductivité ionique a été mesurée par spectroscopie d'impédance complexe. Les résultats obtenus montrent que la conductivité augmente en fonction de la substitution et qu'elle suit la loi d'Arrhenius dans le domaine de température étudié. Aux températures élevées, un changement de l'énergie d'activation est observé. Il a été relié à la nature de la liaison Ca/La–F, et plus précisément à la polarisabilité du lanthane.

1. Introduction

Apatites are a large group of minerals whose main representative is fluoroapatite ($Ca_{10}Fap$), crystallizing mainly in the hexagonal structure (space group $P6_3/m$), where the PO_4^{3-} groups build the framework and the Ca^{2+} ions occupy two non-equivalent sites, $S(1)$ and $S(2)$. Thanks to its stability and flexibility, this structure can accommodate a great variety of substitutions – both cationic and anionic – leading to a wide variety of compounds having different properties, and making them fit for use in various application fields. Hydroxyapatite ($Ca_{10}Hap$), deriving from $Ca_{10}Fap$ by the substitution of OH^- for F^-, is widely used as bone substitutes and coatings on metallic prostheses owing to its good biocompatibility, bioactivity and osteoconductive properties [1–4]. Furthermore, to improve its biological and physicochemical properties, many species contained in biological apatite have been

* Corresponding author.
E-mail address: khaled.bouzouita@ipeim.rnu.tn (K. Bouzouita).

1631-0748/$ – see front matter
http://dx.doi.org/10.1016/j.crci.2014.02.005

incorporated into synthetic Ca_{10}Hap [4]. Apart from biomedical applications, Ca_{10}Hap and Ca_{10}Fap substituted with various ions have been used in catalysis [5], chromatography [6–8] or as adsorbents for the removal of heavy metals and many other species [9–13].

Another class of apatites – rare-earth-based apatites – has gained great interest from researchers for over several decades given their appealing properties. For example, compounds with various compositions, $Ln_{9.33}(XO_4)_6O_2$, $Ln_{10}(XO_4)_6O_3$ and $Ln_{10-x}M_x(XO_4)_6O_{3-x/2}$, where Ln is a rare-earth like La, Nd, etc., M is an alkaline earth like Ca, Sr, etc., and X is either Si or Ge, are extensively investigated thanks to their good ionic conductivity [14–18]. They are considered promising candidates to replace yttria-stabilized zirconia as solid oxide fuel cells (SOFCs) electrolytes at intermediate temperatures [19,20]. Also, oxyapatites doped with rare-earth ions, such as Eu^{3+}, Tb^{3+}, etc. have attracted the researchers' attention for their luminescence properties [21,22]. On the other hand, the compounds with the general formula $Ca_{10-x}Ln_x(PO_4)_{6-x}(SiO_4)_xF_2$ (Ln = La, Nd) have been the subject of both theoretical and experimental studies, because of their potential use as confinement matrices for the minor actinides and long-lived fission products [23–31]. Ardhaoui et al. [32,33], studying the thermodynamic properties of the latter series of compounds, have shown that their enthalpy of formation increased with the increase of the substitution of the pair (Ln^{3+}, SiO_4^{4-}) for the pair (Ca^{2+}, PO_4^{3-}). Furthermore, although a number of studies have been carried out on the structure [34–36] and properties [26–31] of the latter series, to our knowledge, no author has investigated its ionic conductivity.

In order to get a better understanding of the evolution of their properties with the substitution degree, a systematic study of lanthanide-substituted fluoro- and oxyapatites has been undertaken in our laboratory [36–41]. In this paper, we investigate the ionic conductivity of the $Ca_6La_4(PO_4)_2(SiO_4)_4F_2$ and $Ca_4La_6(SiO_4)_6F_2$ samples using impedance spectroscopy.

2. Experimental procedure

2.1. Sample preparation

Samples with the chemical formula $Ca_{10-x}La_x(PO_4)_{6-x}(SiO_4)_xF_2$, with $x = 0$, 4 and 6, were synthesized via a solid-state reaction from $CaCO_3$, CaF_2, La_2O_3, SiO_2, and $Ca_2P_2O_7$. The latter compound was obtained by heating a stoichiometric mixture of $CaCO_3$ and $(NH_4)_2HPO_4$ at 900 °C for 10 h. To avoid the deviation from stoichiometry, lanthanum oxide was calcined at 1000 °C for 24 h just before use, because it is very sensitive to moisture and carbon dioxide from the air [42]. The starting materials in suitable proportions were weighed and thoroughly ground in an agate mortar. Then, they were pressed into pellets, which were firstly heat-treated under a dynamic atmosphere of argon at 900 °C for 12 h, in order to remove the volatile species. After this heat treatment, the pellets were manually crushed and homogenized, and the resulting powders were again uniaxially pressed. According to their SiO_2 content and until a pure phase was obtained, the compacts have undergone one or more heat treatments at a temperature between 1200 and 1400 °C for 12 h under the same atmosphere. The heating rate was 10 °C/min.

After heat treatment, the density (d_{ex}) of a compact was determined from its dimension and weight, and the relative density was calculated using the formula:

$$\rho = \frac{d_{ex}}{d_{theo}} \quad (1)$$

The theoretical density (d_{theo}) was calculated for each composition, taking into account its molecular weight (W), the number of units per unit cell (Z) and the volume of the unit cell, according to the following equation:

$$d_{theo} = \frac{ZW}{A \times a^2 \times c \times \sin 120^\circ} \quad (2)$$

where A is Avogadro's number, and a and c are the lattice parameters.

In the following sections, the compositions with $x = 4$ and 6 will be labelled as Ca_6La_4Fap and Ca_4La_6Fap, respectively.

2.2. Sample characterization

The X-ray diffraction (XRD) patterns of the samples were obtained on a Bruker D8 ADVANCE diffractometer operating with Cu Kα radiation. The samples were scanned in the 2θ range from 20 to 60° with a step size of 0.02° and a counting time of 10 s per step. The lattice parameters were refined by using the Rietveld method.

The MAS–NMR analyses were conducted on ^{31}P and ^{29}Si nuclei using a Bruker 300 WB spectrometer at resonance frequencies of 121.50 and 59.62 MHz, respectively. The spinning rate of the sample at the magic angle was 8 kHz. ^{31}P and ^{29}Si chemical shifts were referenced to external standards of an aqueous solution of 85% H_3PO_4 and tetramethylsilane (TMS), respectively.

Impedance measurements were carried out on samples with $x = 4$ and 6, whose relative density was about 77%, using a Hewlett-Packard 4192-A impedance analyzer, operating at frequencies ranging from 5 to 13 MHz. Silver electrodes were painted on the two faces of the pellets with a silver paste, and then the painted pellets were heated at 300 °C for 1 h.

3. Results and discussion

3.1. Phase identification

Fig. 1 shows the XRD patterns of samples for $x = 0$, 4 and 6. As seen, all the patterns exhibit only the reflections of an apatitic phase, indexed in the hexagonal system (space group $P6_3/m$) based on the fluoroapatite (JCPDS card #00-071-0880). No evidence of any second phase was found, indicating that the samples were single phased.

The insertion of La^{3+} and SiO_4^{4-} within the apatite lattice can be verified by comparing the lattice parameters of the substituted samples with those of Ca_{10}Fap. Both a and c are known to increase when Ca^{2+} and PO_4^{3-} ions are

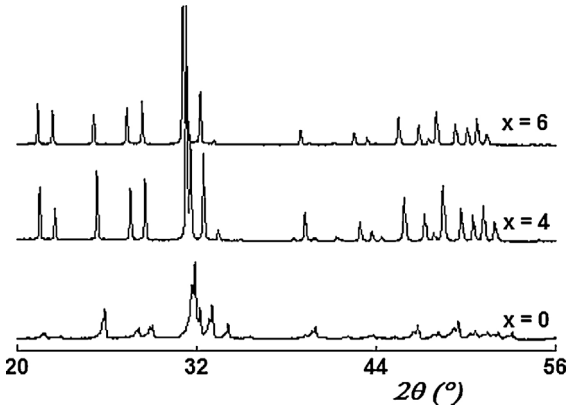

Fig. 1. XRD patterns of $Ca_{10-x}La_x(PO_4)_{6-x}(SiO_4)_xF_2$ samples.

respectively substituted by bigger ones. In agreement with this, it can be seen from Table 1 that the lattice parameters increase with the rise of the substitution degree: the ionic radii of La^{3+} (coord. 9: $r = 1.22$ Å) and Si^{4+} (coord. 4: $r = 0.42$ Å) being bigger than those of Ca^{2+} (coord. 9: $r = 1.18$ Å) and P^{5+} (coord. 4: $r = 0.35$ Å) [43], respectively. That is an evidence of the incorporation of La^{3+} and SiO_4^{4-} into the apatite structure. Compared to those of Ca_4Nd_6F ($a = 9.527(2)$ Å and $c = 7.013(2)$ Å) [34], the lattice parameters of the Ca_4La_6F compound are higher. This is in accordance with the value of the ionic radius of Nd (coord. 9: $r = 1.16$ Å) [43].

The conclusion drawn from the XRD analysis for the substitution of SiO_4^{4-} for PO_4^{3-} can also be evidenced by MAS–NMR analysis. The ^{31}P and ^{29}Si MAS–NMR spectra of the samples are shown in Figs. 2 and 3, respectively. The resolved peaks were assigned according to the literature data [37,38]. For $x = 0$ and 4, the ^{31}P spectra exhibit only a single resonance peak at 2.55 and 1.02 ppm, respectively (Fig. 2), as it is expected from the literature data. The decrease of the isotropic shift would be related to the change of the environment of the PO_4^{3-} groups. Such a phenomenon has already been observed [44]. Also, with the substitution, a broadening of the peak and a decrease of its intensity occurred. The broadening can be associated with the modification of the phosphate group's environment, whereas the intensity decrease is due to the decrease of the phosphorus content in the sample. Similarly, the ^{29}Si NMR spectra of the samples (Fig. 3) show a single resonance peak at −74.53 and −75.84 ppm for $x = 4$ and 6, respectively. This result related to Q° silicate species [45] is in agreement with those obtained for apatites prepared in the La–Si–O system [46]. Therefore, it seems that Si is inserted in the P crystallographic site.

Table 1
Unit cell parameters of $Ca_{10-x}La_x(PO_4)_{6-x}(SiO_4)_xF_2$ samples.

Lattice parameters	$x = 0$	$x = 4$	$x = 6$
a (Å)	9.389(6)	9.562(7)	9.638(4)
c (Å)	6.886(6)	7.040(4)	7.113(2)
V (Å^3)	528.82(3)	557.57(0)	572.27(9)

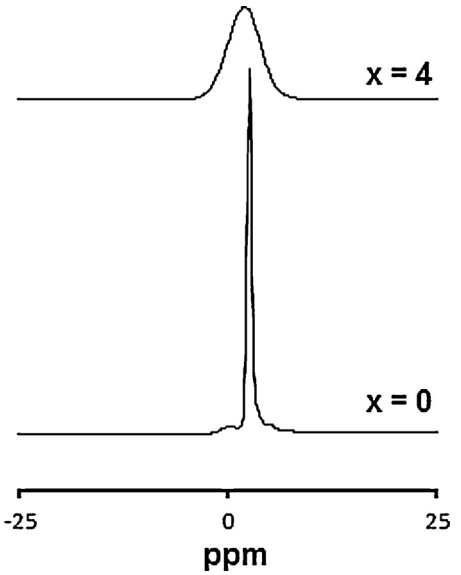

Fig. 2. ^{31}P MAS–NMR spectra of $Ca_{10-x}La_x(PO_4)_{6-x}(SiO_4)_xF_2$ samples.

3.2. Ionic conductivity measurements

The complex impedance spectroscopy of the Ca_6La_4F and Ca_4La_6F samples was measured as a function of the frequency in the 400–800 °C temperature range. The complex impedance plane, Z'' vs Z', plots (not shown here) did not permit to resolve the bulk and boundary semicircles. The total resistance value was determined from the intercept of the semicircular arcs at high frequency with the real axis. Then, the ionic conductivity was deduced from the resistance data using the following relation:

$$\sigma = \frac{e}{sR} \tag{3}$$

where R is the resistance determined from the impedance plots, and e and s are the thickness and area of the sample, respectively.

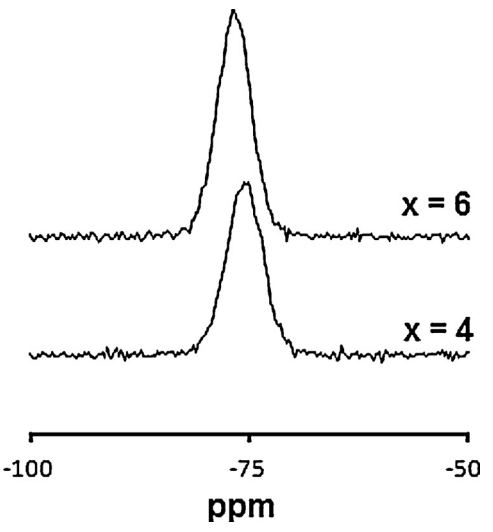

Fig. 3. ^{29}Si MAS–NMR spectra of $Ca_{10-x}La_x(PO_4)_{6-x}(SiO_4)_xF_2$ samples.

In accordance with the conditions indicated above, the obtained values represent the total conductivity. The temperature dependence of the samples' ionic conductivity is shown in Fig. 4 as an Arrhenius-type plot, Log(σT) vs. 1000/T. Just for comparison, the data of $Ca_{10}Fap$ [47] are also represented. It can be seen that with the substitution of (La^{3+}, SiO_4^{4-}) for (Ca^{2+}, PO_4^{3-}):

- the electrical conduction in the materials is a thermally activated process;
- the conductivity increases and the activation energy decreases, Ca_4La_6F has the highest conductivity and the lowest activation energy (Table 2);
- the samples exhibit a change in slope at 717 °C and 620 °C for Ca_6La_4F and Ca_4La_6F, respectively.

However, the ionic conductivity values of 1.07×10^{-7} and 4.14×10^{-6} S·cm^{-1} determined at 800 °C for Ca_6La_4F and Ca_4La_6F, respectively, are lower than that reported for $Ca_{10}Fap$ by Laghzizil et al. (3.35×10^{-5} S·cm^{-1}) [47]. This difference is probably due to the synthesis and sintering conditions used for the different materials. The relative density of our samples was only of about 0.77, while that of $Ca_{10}Fap$ prepared by Laghzizil et al. was 0.90 [47]. The activation energies for conduction were calculated from the slopes of the Arrhenius plots. As seen in Table 2, the activation energy decreases significantly with the substitution. It is worth noting that this decrease is similar to that of the chemical stability of the compounds. Indeed, their enthalpy of formation increases with the substitution degree [33]. Furthermore, according to the shape of the Arrhenius plots, the low-temperature domain is associated with the lowest activation energy. Studying the electrical properties of hydroxyapatites ($M_{10}(PO_4)_6(OH)_2$) and fluoroapatites ($M_{10}(PO_4)_6F_2$) (M = Ca, Pb, Ba), Laghzizil et al. observed that the break occurred only for lead apatites [48].

Like in $Ca_{10}Fap$, the conduction mechanism in our materials should be related to the translational hopping of the fluoride ions along the c-axis of the lattice from ordinary sites to interstitial sites, as these ions are the only candidates for such a conduction process. Thus, the fluoride ions must be able to move to other positions by the formation of thermally activated defects, such as Schottky defects [47], especially as these materials were stoichiometric [36]. With the substitution of (Ca^{2+}, PO_4^{3-}) by (La^{3+}, SiO_4^{4-}), the increase of the conductivity would be due to the expansion of the a-axis, and therefore to the expansion of the anionic tunnel. In addition, the polarizability of La^{3+} (13.07×10^{-30} m^3), higher than that of Ca^{2+} (5.91×10^{-30} m^3) [49], probably played a role in the improvement of the conductivity. Indeed, the conductivity of $M_{10}Fap$ (where M = Ca, Pb, Ba) increases in the order $Ca_{10}Fap < Ba_{10}Fap < Pb_{10}Fap$, although the size of Ba^{2+} is higher than that of Pb^{2+}. With respect to $Ba_{10}Fap$, the higher conductivity of $Pb_{10}Fap$ was attributed to the polarizability of Pb [48], which is higher than that of Ba. Similarly, the conductivity increase in the system $Ca_{10-x}La_x(VO_4)_6O_{1+x/2\cdot1-x/2}$ (where $0 \le x \le 1.5$) was explained by tunnel expansion and La^{3+} polarizability [50]. In our case, in addition to the substitution of La^{3+} for Ca^{2+}, PO_4^{3-} was also substituted by SiO_4^{4-}. As P is more electronegative than Si, with increasing the content of this latter element, the P/Si–O bond is weakened and the O–La one is strengthened. Obviously, the strength of the Ca/La–F bond is affected, thereby facilitating its break. In agreement with this, the structural refinement by the Reitveld method of the compounds with the general formula of $Ca_{10-x}La_x(PO_4)_{6-x}(SiO_4)_xF_2$ ($0 \le x \le 6$) showed that for $Ca_{10}Fap$, the fluoride ions are located at the ideal 2a (0 0 ¼) positions, corresponding to the centers of the triangles formed by Ca(2) atoms. However, with the substitution, especially for the high x values, the F^- ions moved outside their ideal positions. For example, the refined z parameter is of 0.2998(16) for Ca_4La_6Fap [36]. As a result of this shift, there was a weakening of the Ca/La–F bond, thereby facilitating its rupture. Also, the disorder induced by the substitution probably facilitated the diffusion of the F^- ions. Indeed, the investigation of the effect of the substitution on the electronic structure of the $Ca_{10-x}La_x(PO_4)_{6-x}(SiO_4)_xF_2$ ($0 \le x \le 6$) apatites using the DFT method showed that the Ca/LaO_6F polyhedron was more distorted than that of Ca/LaO_9, and the distortion increased with the substitution degree. In addition to the shift of the F^- ions outside the centers of the triangles formed by the Ca/La(2)– atoms when the La content increased, the Ca/La(2)–O bonds were also affected: Ca/La(2)–O(1) and Ca/La(2)–O(3) distances became more elongate and that of Ca/La(2)–O(2) became shorter [51]. Furthermore, the structural refinement of this series by the Rietveld method has shown that the La^{3+} ions occupied preferentially the sites (2) [36].

The break in the Arrhenius plots is usually related to a phase transition [52] or to a change in the conduction mechanism [53]. However, in the present case, no phase change was observed in the investigated temperature

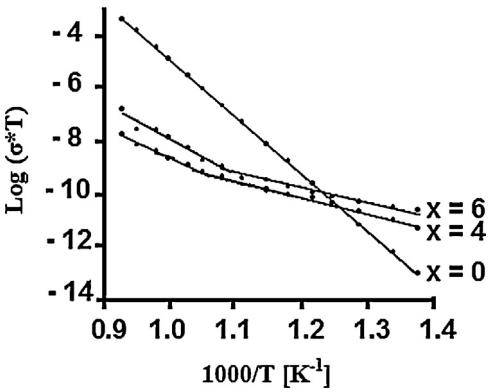

Fig. 4. Plot of Log σT (S·K·cm^{-1}) versus 1000/T (K^{-1}) for $Ca_{10-x}La_x(PO_4)_{6-x}(SiO_4)_xF_2$ samples: $x = 0$ [47]; $x = 4$ and 6 (present work).

Table 2
Activation energy values of $Ca_{10-x}La_x(PO_4)_{6-x}(SiO_4)_xF_2$ samples.

Samples	$x = 0$ [47]	$x = 4$	$x = 6$
E_a (eV)	1.86	1.07 0.54	1.01 0.46

range, and no change in the conduction mechanism can be suspected, the F^- ions being the only charge carriers in the absence of cationic vacancies [36]. Like for lead fluoroapatite, the break in the Arrhenius curve is related to the nature of the Ca/La–F bond, i.e. to the polarizability of the atoms located in the *S*(2) sites, as it has been suggested by Laghzizil et al. [47]. The decrease of the breakpoint temperature when *x* varied from 4 to 6 could be related to the increase in the conductivity. The same behavior was observed with Pb_{10}Hap and Pb_{10}Fap, the fluoride ions being more mobile than the protons. Indeed, the change of the temperature's slope occurs at 390 °C for Pb_{10}Fap, while it occurs at 480 °C for Pb_{10}Hap [48].

4. Conclusion

$Ca_6La_4(PO_4)_2(SiO_4)_4F_2$ and $Ca_4La_6(SiO_4)_6F_2$ were synthesized by a solid-state reaction. They were characterized by X-ray diffraction and nuclear magnetic resonance spectroscopy. Their ionic conductivity was measured by impedance spectroscopy. The obtained results indicated that:

- the conduction is due to the mobility of F^- ions along the *c*-axis of the lattice. The increase in conductivity with the substitution is caused by the widening of the tunnel and the weakening of the Ca/La–F bond;
- the Arrhenius curves show a change in slope, which was related to the polarizability of the lanthanum. The decrease in the temperature at which the break occurs is attributed to the increase of the conductivity.

References

[1] M. Jarcho, Clin. Orthop. Relat. Res. 157 (1981) 259.
[2] K. De Groot, Bioceramics of calcium phosphate, CRC Press, Boca Raton, FL, USA, 1983.
[3] L.L. Hench, J. Am. Ceram. Soc. 74 (1991) 1487.
[4] M. Vallet-Regí, J.M. González-Calbet, Prog. Solid State Chem. 32 (2004) 1.
[5] H. Monma, J. Catal. 75 (1982) 200.
[6] S. Schubert, R. Freitag, J. Chromatogr. A 1142 (2007) 106.
[7] L. Dattolo, E.L. Keller, G. Carta, J. Chromatogr. A 1217 (2010) 7573.
[8] A. Benmoussa, C. Delaurent, J.-L. Lacout, P.-R. Loiseau, M. Mikou, J. Chromatogr. A 731 (1996) 153.
[9] S. Baillez, A. Nzihou, D. Bernache-Assolant, E. Champion, P. Sharrock, J. Hazard. Mater. A139 (2007) 443.
[10] F. Yuan, G. Ji-Lai, Z. Guang-Ming, N. Qiu-Ya, Z. Hui-Ying, N. Cheng-Gang, D. Jiu-Hua, Y. Ming, Chem. Eng. J. 162 (2010) 487.
[11] S. Bailliez, A. Nzihou, E. Bèche, G. Flamant, Process Saf. Environ. Protect. 82 (B2) (2004) 175.
[12] M. Mourabet, A. El Rhilassi, H. El Boujaady, M. Bennani-Ziatni, R. El Hamri, A. Taitai, J. Saudi Chem. Soc. (2012), http://dx.doi.org/10.1016/j.jscs.2012.03.003.
[13] C. Verwilghen, S. Rio, A. Nzihou, D. Gauthier, G. Flamant, P.J. Sharrock, J. Mater. Sci. 42 (2007) 6062.
[14] S. Nakayama, T. Kageyama, H. Aono, Y. Sadaoka, J. Mater. Chem. 5 (1995) 1801.
[15] S. Nakayama, H. Aono, Y. Sadaoka, Chem. Lett. 6 (1995) 431.
[16] S. Nakayama, M. Sakamoto, J. Eur. Ceram. Soc. 18 (1998) 1413.
[17] S. Nakayama, M. Higuchi, J. Mater. Sci. Lett. 20 (2001) 913.
[18] H. Arikawa, H. Nishiguchi, T. Ishihara, Y. Takita, Solide State Ionics 136 (2000) 31.
[19] Y. Masubuchi, M. Higuchi, T. Takeda, S. Kikkawa, J. Alloys Compds 408 (2006) 641.
[20] H. Yoshioka, J. Alloys Compds 408 (2006) 649.
[21] L. Boyer, B. Piriou, J. Carpena, J.-L. Lacout, J. Alloys Compds 311 (2000) 143.
[22] J. Lin, Q. Su, J. Alloys Compds 210 (1994) 159.
[23] V. Louis-Achille, L. Dewindt, M. Defranceschi, Int. J. Quantum Chem. 77 (2000) 991.
[24] C. Meis, J.D. Gale, L. Boyer, J. Carpena, D. Gosset, J. Phys. Chem. 104 (2000) 5380.
[25] C. Meis, J. Nucl. Mater. 289 (2001) 167.
[26] N. Dacheux, N. Clavier, A. Robisson, O. Terra, F. Audubert, J. Lartigue, C. Guy, C. R. Chimie 7 (2004) 1141.
[27] O. Terra, N. Dacheux, F. Audubert, R. Podor, J. Nucl. Mater. 352 (2006) 224.
[28] O. Terra, F. Audubert, N. Dacheux, C. Guy, R. Podor, J. Nucl. Mater. 354 (2006) 49.
[29] O. Terra, F. Audubert, N. Dacheux, C. Guy, R. Podor, J. Nucl. Mater. 366 (2007) 70.
[30] E. Du Fou de Kerdaniel, N. Clavier, N. Dacheux, O. Terra, R. Podor, J. Nucl. Mater. 362 (2007) 451.
[31] N. Dacheux, E. Du Fou De Kerdaniel, N. Clavier, R. Podor, J. Aupiais, J. Nucl. Mater. 404 (2010) 33.
[32] K. Ardhaoui, M.V. Coulet, A. Ben Chérifa, J. Carpena, J. Rogez, M. Jemal, Thermochim. Acta 444 (2006) 190.
[33] K. Ardhaoui, Doctoral Thesis, University of Tunis, Tunisia, 2006.
[34] J. Carpéna, L. Boyer, M. Fialin, J.-R. Kiénast, J.-L. Lacout, C. R. Acad. Sci. Paris, Ser. IIa 333 (2001) 373.
[35] L. Boyer, J.-M. Savariault, J. Carpena, J.-L. Lacout, Acta Crystallogr. C 54 (1998) 1057.
[36] H. Njema, K. Boughzala, H. Boughzala, K. Bouzouita, J. Rare Earths 31 (2013) 897.
[37] K. Boughzala, E. Ben Salem, F. Kooli, P. Gravereau, K. Bouzouita, J. Rare Earths 26 (2008) 483.
[38] K. Boughzala, S. Nasr, E. Ben Salem, F. Kooli, K. Bouzouita, J. Chem. Sci. 121 (2009) 283.
[39] K. Boughzala, N. Gmati, K. Bouzouitahttp Ben Cherifa, P. Gravereau, C. R. Chimie 13 (2010) 1377.
[40] A. Hassine, N. Jaba, G. Panczer, K. Bouzouita, C. R. Chimie 13 (2010) 1460.
[41] N. Gmati, K. Boughzala, A. Chaabène, N. Fattah, K. Bouzouita, C. R. Chimie 16 (2013) 712.
[42] P.J. Panteix, I. Julien, D. Bernache-Assollant, P. Abelard, J. Mater. Chem. Phys. 95 (2006) 313.
[43] R.D. Shannon, Acta Crystallogr. 32 (1976) 751.
[44] A. Laghzizil, N. Elherch, A. Bouhaouss, G. Lorent, T. Coradin, J. Livage, Mater. Res. Bull. 36 (2001) 953.
[45] G. Engelhardt, D. Michel, High resolution solid-state NMR of silicates and zeolites, John Wiley, Norwich, UK, 1987.
[46] J.E.H. Sansom, J.R. Tolchard, M.S. Islam, D. Apperley, P.R. Slater, J. Mater. Chem. 16 (2006) 1410.
[47] A. Laghzizil, A. Bouhaouss, M. Ferhat, P. Barboux, R. Morineau, J. Livage, Adv. Mater. Res. 1–2 (1994) 479.
[48] A. Laghzizil, N. El Herch, A. Bouhaouss, G. Lorente, G. Macquete, J. Solid State Chem. 156 (2001) 57.
[49] Y. Marcus, Ion Properties, Marcel Dekker, New York, 1997.
[50] H. Benmoussa, M. Mikou, A. Bensaoud, A. Bouhaouss, R. Morineaux, Mater. Res. Bull. 35 (2000) 369.
[51] H. Njema, M. Debbichi, K. Boughzala, M. Said, K. Bouzouita, Mater. Res. Bull. 51 (2014) 210.
[52] T. Naddari, H. El Feki, J.M. Savariault, P. Salles, A. Ben Salah, Solid State Ionics 158 (2003) 157.
[53] L. Léon-Reina, J.M. Porras-Vázquez, E.R. Losilla, M.A.G. Aranda, J. Solid State Chem. 180 (2007) 1250.